

Vapor Growth and Tunable Lasing of Band Gap Engineered Cesium Lead Halide Perovskite Micro/Nanorods with Triangular Cross Section

Hong Zhou,[†] Shuangping Yuan,[†] Xiaoxia Wang,[†] Tao Xu,[‡] Xiao Wang,^{*,†} Honglai Li,[†] Weihao Zheng,[†] Peng Fan,[†] Yunyun Li,[†] Litao Sun,[‡] and Anlian Pan^{*,†}

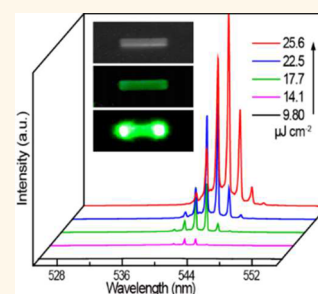
[†]Key Laboratory for Micro-Nano Physics and Technology of Hunan Province, State Key Laboratory of Chemo/Biosensing and Chemometrics, and School of Physics and Electronics, Hunan University, Changsha 410082, P. R. China

[‡]SEU-FEI Nano-Pico Center, Key Lab of MEMS of Ministry of Education, Southeast University, Nanjing 210096, P. R. China

S Supporting Information

ABSTRACT: Although great efforts have been devoted to the synthesis of halide perovskites nanostructures, vapor growth of high-quality one-dimensional cesium lead halide nanostructures for tunable nanoscale lasers is still a challenge. Here, we report the growth of high-quality all-inorganic cesium lead halide alloy perovskite micro/nanorods with complete composition tuning by vapor-phase deposition. The as-grown micro/nanorods are single-crystalline with a triangular cross section and show strong photoluminescence which can be tuned from 415 to 673 nm by varying the halide composition. Furthermore, these single-crystalline perovskite micro/nanorods themselves function as effective Fabry–Perot cavities for nanoscale lasers. We have realized room-temperature tunable lasing of cesium lead halide perovskite with low lasing thresholds ($\sim 14.1 \mu\text{J cm}^{-2}$) and high Q factors (~ 3500).

KEYWORDS: cesium lead halide perovskites, triangular micro/nanorods, tunable lasers, vapor-phase growth



Lead halide perovskite materials have received intensive attention owing to their outstanding characteristics such as long electron–hole diffusion lengths, tunable bandgap, high carrier mobility, and low trap-state density, which lead to fascinating applications in optoelectronics, such as high-efficiency solar cells, electroluminescence devices, and lasers.^{1–11} Research interest in all-inorganic cesium lead halide perovskites (CsPbX_3 , X = Cl, Br, and I) has increased substantially over the past years.^{12–14} Compared to the organic components, all-inorganic perovskites can overcome the limitation of being vulnerable to the moisture, heat, oxygen, light, and electrical field.^{15–17}

For the applications in high-performance optoelectronic devices working over a large range of wavelengths, band gap engineering of all-inorganic perovskites is highly desirable and critical.^{18–20} Creating a mixed alloy system with variable chemical compositions has been proved to be an effective strategy for the band gap engineering of semiconductor nanomaterials.^{21,22} Since the band gap of the CsPbX_3 perovskites depends on the hybridization states between cation Pb and anion X orbitals,^{23,24} it is of vital importance to control these perovskites with modulated composition for creating tunable optoelectronic devices.

In the past two years, many efforts have been devoted to the solution-phase synthesis of CsPbX_3 perovskite nanocrystals and quantum dots with tunable compositions and optical properties.^{12,23,25} Yang and co-workers reported a fine composition control in a CsPbX_3 perovskite nanowire system using a wet-chemistry anion-exchange reaction method.²⁶ It is well-known that one-dimensional (1D) semiconductor nanostructure can act as good gain media and optical cavities.^{27,28} Lasing has been observed from the solution-phase grown single-crystalline CsPbBr_3 nanowires, indicating their promising potential applications in integrated photonics devices and systems.^{29,30} Compared with a solution-phase method, vapor-phase deposition has been generally used to synthesize high-quality optoelectronic materials and could offer an alternative flexible and convenient method to grow semiconductor nanostructures with high-quality and tunable composition and band gaps.^{9,21,31} For 1D structures, vapor-phase deposition has been demonstrated as an excellent approach to achieve axial nanowire heterostructures and band gap grade semiconductor nanostructures.

Received: November 2, 2016

Accepted: December 27, 2016

Published: December 30, 2016

tures due to the full controllable parameters. Moreover, optoelectronic devices may be fabricated directly on the growth substrates, which provides the potential for large-scale integrated devices. While the most of the research has focused on solution synthesis routes, vapor-phase synthesis of all-inorganic perovskite nanostructures have only been developed very recently. For example, Xiong *et al.* has successfully synthesized high-quality CsPbX₃ nanoplatelets using vapor-phase method, and low-threshold lasing based on the whispering gallery mode is observed in individual perovskite plates.³² Very recently, single-composition perovskite nanowires of CsPbI₃, CsPbBr₃, and CsPbCl₃ synthesized by vapor growth have also been reported with strong light–matter interactions observed,³³ but to the best of our knowledge, vapor-phase growth of composition-tuned all-inorganic cesium lead halide perovskite nanowires has not yet been achieved.

Herein, we report a vapor-phase growth of high-quality cesium lead halide micro/nanorods with tunable compositions. These micro/nanorods are high-quality single crystals with well-defined triangular facets and a wavelength completely tuned PL emission covering almost the whole visible spectral region. Since the triangular cross section has been reported manifesting an uniformly high-Q factor in a wide spectral range than that from other shapes, 1D nanostructures with triangular cross sections are more suitable for tunable laser applications.³⁴ Therefore, we evaluated the lasing properties of these alloy perovskite micro/nanorods. The as-grown triangular rods with triangular cross section can act as high-quality Fabry–Perot (FP) cavities and can realize high-quality multicolor lasing under laser pumping with very low pumping threshold and high-quality factor. These remarkable results would lead to potential promising applications in integrated photonics and optoelectronic devices and systems.

RESULTS AND DISCUSSION

The cesium lead halide perovskite triangular micro/nanorods were grown on SiO₂/Si substrates *via* an improved vapor deposition method. Briefly, an alumina boat containing of a mixture of CsX and PbX₂ powders was placed at the heating zone of a home-built vapor deposition system (Figure S1). Several pieces of SiO₂/Si substrate were placed at the downstream of the quartz tube to grow the CsPbX₃ samples. The equilibrium partial pressure of CsX and PbX₂ can be precisely controlled by systematically varying the temperature of the precursors with fully tunable compositions. As shown in the scanning electron microscopy (SEM) image (Figure 1a,b), perovskite micro/nanorods with the length of about 2–20 μm were achieved on the SiO₂/Si substrate. The majority of the micro/nanorods is found to have triangle cross sections. Tetrahedron products are also observed in all compositions. Elemental analysis from energy dispersive X-ray spectrum (EDX) on individual triangular rods (Figure S2) confirms the formation of CsPbX₃ alloy. SEM image and EDX mapping of a CsPbBr₃ nanorod (Figure 1c) show uniform spatial distribution of Cs, Pb, and Br throughout the nanorods. The structure of as-grown CsPbX₃ triangular micro/nanorods was examined *via* X-ray diffraction (XRD) (Figure 1d). All the sharp diffraction peaks of the products can be indexed to the perovskite phase of CsPbX₃. These patterns revealed that a tetragonal phase CsPbCl₃ and a monoclinic phase CsPbBr₃ are formed. For CsPbI₃, a phase-pure perovskite structure was not obtained in our experiments. CsPbI₃ is not stable as a perovskite phase at room temperature, but is stable at high temperature (~130

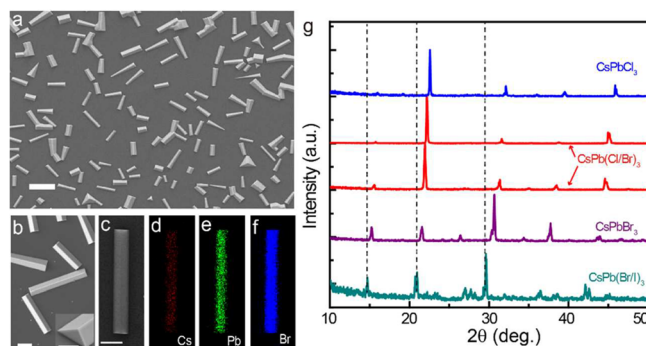


Figure 1. (a) SEM image of as-grown CsPbBr₃ perovskite nanostructures (scale bar, 10 μm). (b) A magnified SEM image of the micro/nanorods (scale bar, 1 μm). The inset is an enlarged tilt view of a perovskite nanorod, showing a triangular cross section and a smooth end facet (scale bar, 400 nm). (c) A typical SEM image of an individual CsPbBr₃ nanorod and (d–f) corresponding EDX mapping, showing uniform spatial distribution of Cs, Pb, and Br elements (scale bar, 1 μm). (g) XRD patterns of the as-grown CsPbX₃ (X = Cl, Cl/Br, Br, and I/Br) mixed halide systems.

°C).³⁵ The obtained CsPbI₃ may experience a phase transition during the sample cooling or over the course of the measurement.³⁶ In addition, the diffraction peaks from bottom to top gradually shift toward large angles, which can be explained by the lattice contraction caused by the decreasing of halide ion radius from I[−] to Cl[−]. Figure 2a clearly shows that

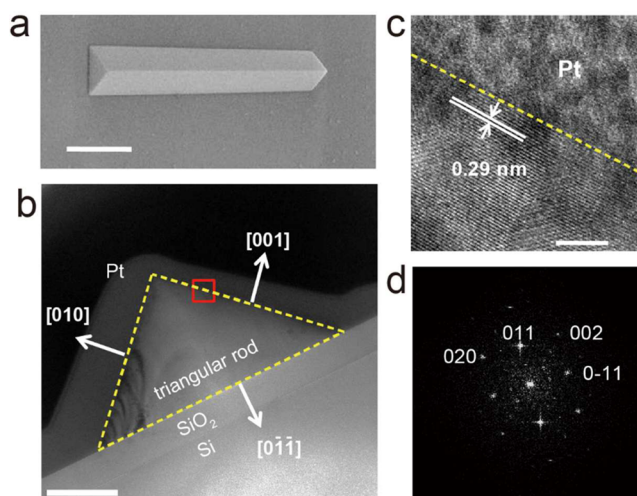


Figure 2. (a) FIB-SEM micrograph of a CsPbBr₃ triangular rod (scale bar, 2 μm). (b) A TEM image of the cross section of the rod which was cut perpendicular to the length of the wire by FIB (scale bar, 500 nm). HRTEM images of the region marked with the red square in (b) are shown in (c), and the corresponding FFT pattern is shown in (d) (scale bar, 5 nm).

the rod has triangle cross sections with well-defined and smooth surfaces. As the as-grown triangular rods are firmly connected with substrates, it is not easy to directly disperse them on Cu grids to carry out the additional structure analyses. For high-resolution transmission electron microscopy (HRTEM) experiments, CsPbBr₃ triangular rod was cut by a focused ion beam (FIB) system. A TEM image of the cross section of the triangular rod is shown in Figure 2b. The edge (marked by a red square) is further examined with HRTEM. The HRTEM images (Figure 2c) demonstrate that the lattice

spacing of the triangular rod is approximately 0.29 nm, corresponding to the (200) lattice plane of monoclinic CsPbBr_3 .³⁷ The corresponding fast Fourier transform (FFT) pattern (Figure 2d) matches the diffraction data. Based on these TEM characterizations, we can conclude that the triangular rod is a single-crystal with a growth direction along the [100] direction.

The growth temperature plays a key role for the formation of these triangular micro/nanorods. CsPbX_3 can crystallize in four types of crystal structures, including monoclinic, tetragonal, orthorhombic, and cubic polymorphs.³⁷ In CsPbX_3 nanostructures, the formation of cubic phase was usually attributed to large surface energy and high growth temperature.^{32,38} During the growth of triangular cross section perovskite micro/nanorods, we found that cubic phase nanoplates were formed at high growth temperatures, while monoclinic phase CsPbBr_3 rods were formed at low growth temperatures (Figure S3). According to the density functional theory (DFT) calculations, the surface free energy of (100) planes is lower than (110) and (001) planes.³⁹ So the rods tend to grow along the [100] direction. The role of the amorphous SiO_2 in the growth mechanism is still unclear. One reasonable explanation is that having a (011) surface interface with SiO_2 can minimize the surface energy. With the (011) plane in parallel with the substrate and the [100] direction as the growth direction, the triangular rods morphology is formed.

Room-temperature photoluminescence (PL) properties of these as-grown samples were investigated based on a confocal optical microscope. Figure 3a shows the luminescence images of the as-grown composition tunable CsPbX_3 triangular rods under the excitation of a focused 375 or 488 nm continuous wave (CW) laser at room temperature. The emission color of the CsPbX_3 samples changes from violet to red with the X varying from Cl to Br/I. In addition, optical waveguide is observed in these images as bright light emitting from both ends of these rods, which indicates that these triangular rods themselves form high-quality optical cavities. Figure 3b shows the corresponding normalized *in situ* PL spectra of the exhibited composition modulated CsPbX_3 triangular rods excited by a 488 nm laser source (see Optical Characterization section) at room temperature. All samples show single emission bands with the spectral peaks shifted from 415 nm (for pure CsPbCl_3) to 673 nm (for $\text{CsPb}(\text{Br}/\text{I})_3$), which covers almost the whole visible range.

As shown in Figure 3b, the CsPbCl_3 triangular rod shows a strong and narrow emission peak at 415 nm with a full width at half-maximum (fwhm) of ~ 17 nm (122 meV). The fwhm values of CsPbBr_3 (peak centered at 534 nm) and $\text{CsPb}(\text{Br}/\text{I})_3$ (peak centered at 673 nm) are increased to ~ 22 nm (94 meV) and ~ 32 nm (82 meV), respectively. The peak positions and the fwhm values are obtained by Gaussian fitting of the detected PL spectra. The fwhm values of the vapor method obtained CsPbX_3 rods (17–32 nm) are all smaller than that of the CsPbX_3 nanowires or nanocrystals synthesized by the solution-phase method, which also supports the argument of high crystal quality of the as-grown samples.²⁵ Figure 3c plots the band gap variations of the achieved CsPbX_3 rods as a function of chemical composition. The filled triangles are the experimental results obtained from the PL peak position and EDX composition analysis. The solid lines are the fitted values according to the special-quasirandom-structures (SQS) calculation.⁴⁰ Significantly, the experimental data are well consistent with the calculated results of SQS, demonstrating that the

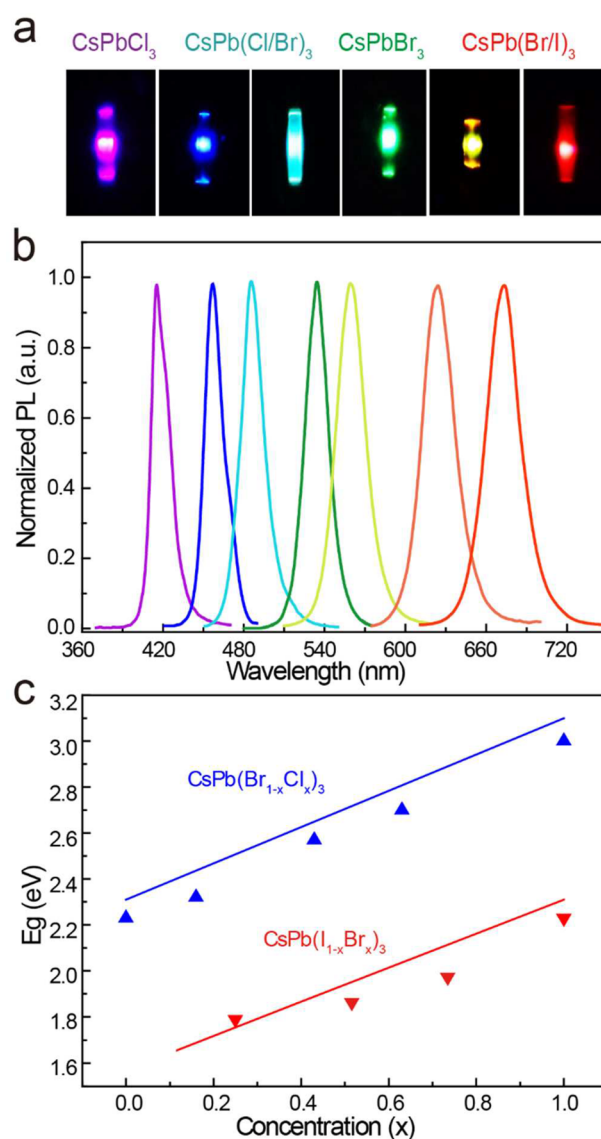


Figure 3. (a) Real-color image of the band gap engineered triangular rod under local laser excitation. (b) PL spectra and (c) band gaps of the alloy triangular rods. The solid triangles are the experimental data, and the solid lines are fitted by SQS calculation at nine different concentrations.

observed single PL emissions are all originated from the near band-edge emission, without any defect-related emission bands. Based on the above results and analysis, we have succeeded in achieving the vapor growth of bandgap engineered all-inorganic cesium lead halide perovskite triangular micro/nanorods with high crystal quality and PL tunability within the wide visible spectral region.

To further demonstrate the application for tunable lasing, using far-field optical microscopy under ambient conditions, a femtosecond pulsed laser beam was focused to a size larger than the triangular rod (Figure 4a) in order to make the energy of the pump source uniform and acquire enough gain from the rod. Figure 4b displays the excitation fluence-dependent PL spectra of the CsPbBr_3 triangular rod. The spontaneous emission spectrum is centered at 538 nm and shows a weak intensity with a fwhm of 15 nm (60 meV) when the excitation fluence is $< 14.1 \mu\text{J cm}^{-2}$. When the excitation fluence increases over $14.1 \mu\text{J cm}^{-2}$, a set of sharp peaks emerge at the low-

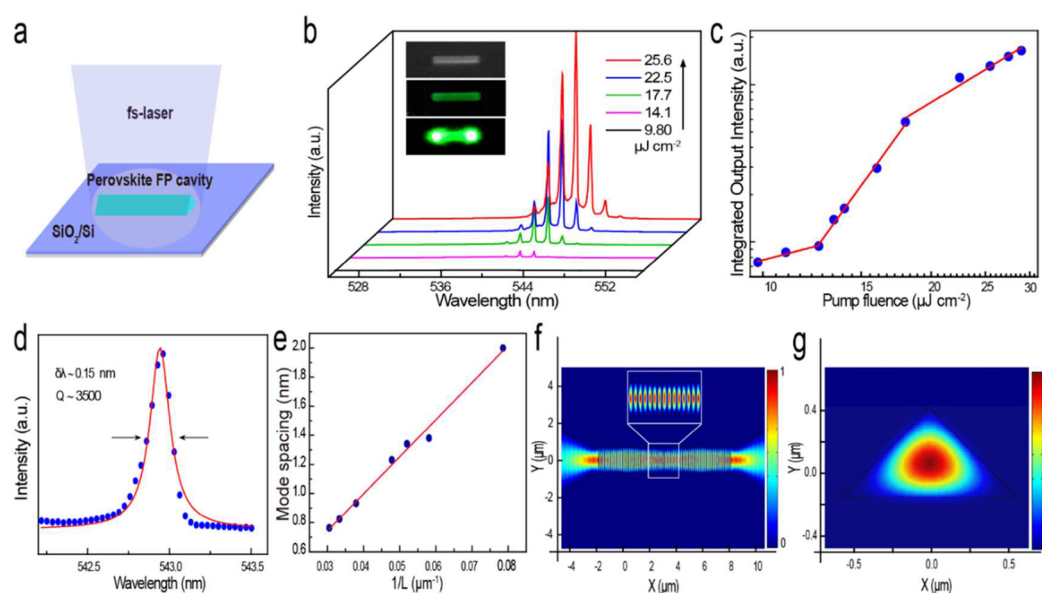


Figure 4. (a) Schematic of a CsPbX₃ nanorod on SiO₂/Si substrate pumped by a fs-laser excitation. (b) Triangular rod emission spectra around the lasing threshold; inset: optical image (up) of a single triangular rod; the middle and right: images show the triangular microrod emission below and above P_{Th} , respectively. (c) Nonlinear response of laser output power with increasing pump fluence. (d) A Lorentz fitting (solid red line) of a lasing oscillation mode (blue circles). (e) The mode spacing is extracted out and plotted as a function of the inverse of the length of rods. (f) 2D electric field intensity distribution at the triangular cross-section of the rod performed by FDTD method. (g) FDTD simulation of 2D normalized electric field intensity distribution ($\lambda = 543$ nm, $n = 2.53$), defining a FP standing-wave cavity mode.

energy side of the emission spectrum around 543 nm and grow rapidly with sequentially increased pumping, which reveals the occurrence of a lasing action from the rod under high excitation fluence. The inset of Figure 4b shows the bright-field optical microscopy image (top) and emission images at low (middle) and high (bottom) excitation fluence of a typical CsPbBr₃ triangular rod. Compared with the uniform emission from the entire triangular rod under low excitation fluence, a strong emission was observed at both ends with the high excitation fluence pumping, indicating the transition from random spontaneous emission to directional stimulated radiation. Figure 4c shows the excitation fluence-dependent output intensity of the triangular rod. The plot clearly exhibits nonlinear behavior (a typical “S”-curve shape)⁴¹ and gives a threshold of $P_{Th} \sim 14.1 \mu\text{J cm}^{-2}$, which also clearly reveals the process of the transition from original spontaneous emission *via* amplified spontaneous emission to finally stimulated radiation with the increasing of the excitation fluence. Generally, the quality factor (Q) indicates the performance of the nanostructure cavity and can be estimated by the spectral profile of the main lasing mode, which can be calculated with the relationship of $Q = \lambda/\delta\lambda$, where λ is the wavelength of the lasing mode and $\delta\lambda$ is the fwhm of this mode.^{9,20} It should be noted that the fwhm of the dominating lasing mode ($\delta\lambda$) at 543 nm is only ~ 0.155 nm (fitted by Lorentz function, see Figure 4d), which corresponds to a Q factor of ~ 3500 . It is three times higher than that of the recently reported value from the solution-phase synthesized all-inorganic CsPbBr₃ nanowires. Two main factors are believed to contribute to the ultrahigh Q of these all-inorganic CsPbBr₃ rods.²⁹ On one hand, the structure shows very smooth and flat end facets with a well-defined triangular cross-section. Importantly, the triangular cross-section structure is confirmed to have good optical confinement from the later simulation result, which is believed to be of great importance to form a high-quality FP type

resonant cavity.^{42,43} On the other hand, the high Q value also can be ascribed to the excellent crystalline properties of the as-synthesized all-inorganic CsPbBr₃ micro/nanorods due to the relatively high reaction temperature during the CVD growth process. It also should be noticed that the quality factor also depends on the dimensions of the cavity, that is, bigger resonators provide a higher Q in general.

For a FP resonator cavity, the lasing mode spacing decreases with the increasing length of the cavity according to the relation $\Delta\lambda = \lambda^2(2n_g L)^{-1}$, where $\Delta\lambda$ is the mode spacing, λ is the wavelength of the light, n_g represents the group refractive index, and L is the length of the triangular rod.^{44,45} In our experiments, tens of CsPbBr₃ triangular rods were examined, and $\sim 90\%$ of them show lasing action at high excitation fluence, with the lasing threshold varying from $2.1 \mu\text{J cm}^{-2}$ to $15 \mu\text{J cm}^{-2}$. The lasing threshold is relatively low and comparable to the results of previously reported perovskite nanostructures lasing, which is mainly due to the low Auger recombination losses and the good crystalline quality of perovskite structures.²⁹ In addition, a group refractive index n_g of ~ 5.8 is extracted out through the fitting (see Figure 4e), which is in agreement with previous studies, suggesting the achievement of FP modes lasing.²⁹

The formation of the FP mode resonance cavity in the rod can be further confirmed by the electrical field distribution simulation. Figure 4f,g shows the normalized two-dimensional (2D) electric field intensity distribution in the cross-section along the length and the triangular cross-section of a rod *via* numerical simulation by Comsol Multiphysics, respectively. The result clearly shows the optical field is well confined in the rod, therefore, preferred mode profiles in the rod are reflected back and forth between the two end facets to form a standing-wave and finally leak out at the end facets, as in the simulation result in Figure 4g, indicating a typical axial FP type cavity

resonance.⁴⁶ The similar phenomena have also been observed in triangular-prism-like CdS.²⁷

Figure 5a shows the wavelength-tunable lasing from 428 to 668 nm of the as-grown band gap engineered cesium lead

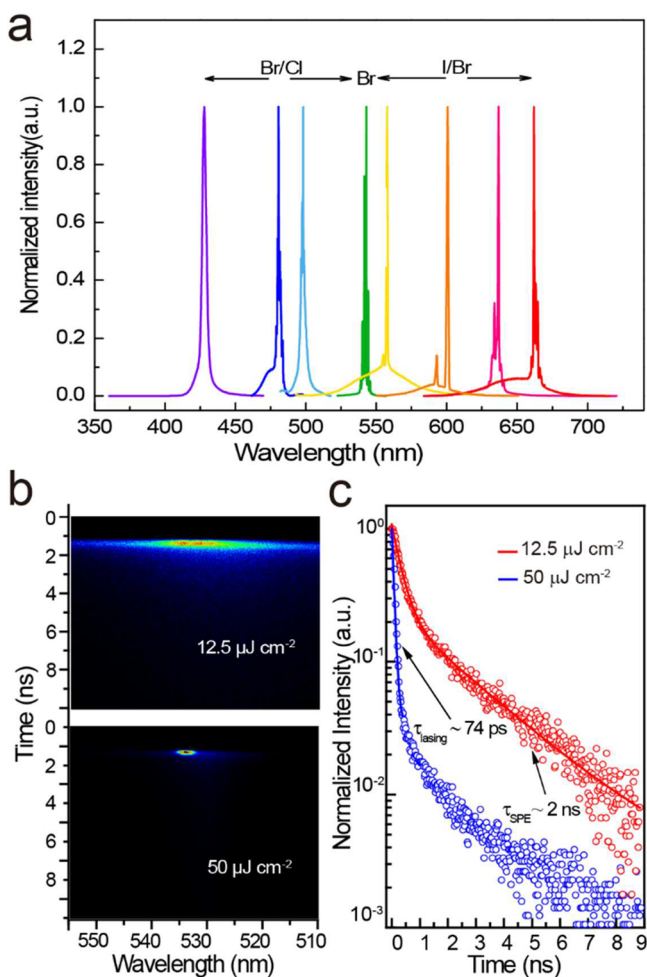


Figure 5. (a) Broad wavelength-tunable lasing at room temperature from triangular rod lasers of CsPbX₃ perovskite. (b) Streak-camera images of single triangular rod when the pump fluence below ($P \sim 12.5 \mu\text{J cm}^{-2}$, top) and above ($P \sim 50 \mu\text{J cm}^{-2}$, bottom) P_{Th} . (c) TRPL decay kinetics after photoexcitation with different pump fluence.

halide perovskite triangular rods at room temperature. Lasing thresholds for CsPb(Br_{1-x}Cl_x)₃ and CsPb(Br_xI_{1-x})₃ are higher than pure CsPbBr₃ samples. It is worth noting that lasing below 480 nm has never been achieved before in organic–inorganic lead halides perovskites, due to the high trap density reported in recently literature.⁵ In addition, the fwhm of the lasing peaks at 496 and 637 nm is only 0.25 and 0.45 nm, respectively, corresponding to Q factors of about ~ 1980 and ~ 1450 (see Figure S4). Although the Q factors for CsPb(Br_{1-x}Cl_x)₃ and CsPb(Br_xI_{1-x})₃ are lower than that of the pure CsPbBr₃ samples, it is still two times larger compared to the previous results.

Time-resolved photoluminescence (TRPL) measurements were used to further prove the occurrence of the lasing in the triangular rod cavities. Figure 5b shows the representative streak camera images of the detected PL from one end of a CsPbBr₃ triangular rod when the excitation fluence is below

($12.5 \mu\text{J cm}^{-2}$, $P = 0.88 P_{\text{Th}}$) and above ($50 \mu\text{J cm}^{-2}$, $P = 3.5 P_{\text{Th}}$) the lasing threshold, respectively. Clearly, spontaneous emission with a broad emission band and longer decay time dominates the emission process below the lasing threshold, and stimulated emission with a much narrower emission band and an ultrashort decay time dominates the process above the lasing threshold. Figure 5c plots the decay curves at the excitation fluence of $12.5 \mu\text{J cm}^{-2}$ and $50 \mu\text{J cm}^{-2}$, respectively, from which the lifetimes τ can be obtained. For the excitation fluence below the threshold ($12.5 \mu\text{J cm}^{-2}$), the spontaneous emission lifetime is as long as $\tau_{\text{SPE}} = 2$ ns. While for the excitation fluence above the threshold ($50 \mu\text{J cm}^{-2}$, Figure 5c, blue trace), an ultrashort emission lifetime of $\tau_{\text{lasing}} = 74$ ps is observed, which further demonstrates the transition from spontaneous emission to stimulated emission.^{47–49}

CONCLUSIONS

In summary, all-inorganic cesium halide perovskite CsPbX₃ micro/nanorods were synthesized *via* a vapor growth method. The as-grown CsPbX₃ micro/nanorods are a single crystalline perovskite structure with ultrasmooth surface and with well-defined triangular facets and show intense spontaneous emission at room temperature. Moreover, these high-quality triangular micro/nanorods can act as ideal FP optical cavities, which is further confirmed by numerical calculations. With these single-crystal perovskite triangular micro/nanorods, we have achieved room-temperature optically pumped tunable lasing covering almost the whole visible spectral region with low lasing thresholds and high-quality factors. These results suggest the all-inorganic cesium halide perovskite CsPbX₃ triangular micro/nanorods could be more promising candidates for use in integrated photonic and optoelectronic devices.

EXPERIMENTAL SECTION

Synthesis of CsPbX₃ Triangular Micro/nanorods and Structural Characterization. The compounds CsPbX₃ perovskite triangular micro/nanorods were synthesized by vapor-phase approach. An alumina boat loaded with mixed powder of CsX and PbX₂ was put inside the heating center of a quartz tube mounted in a furnace (OTF-1200X). Considering the vapor pressure of these materials is different, the molar ratio of CsX and PbX₂ was set to 2:1. Several pieces of Si wafers (with 280 nm SiO₂) were placed at the downstream of the quartz tube. Before heating, the quartz tube was pumped down; high purity Ar (99.999%) was introduced into the tube and maintained the pressure at 300 Torr. Then the furnace was heated at a rate of 30 °C/min from room temperature to a setting temperature at 570–600 °C. The temperature of the substrates was set at approximately 300–400 °C. Continuing the growth for 15 min, the furnace was naturally cooled down to room temperature. The crystalline structure of the triangular micro/nanorods was characterized by XRD (D/max 2500). The *in situ* EDX spectra of the samples were characterized by scanning electron microscopy (Hitachi S-4800). Further structural analyses were carried out by a transmission electron microscope (FEI Titan 80–300 operated at 300 kV) after the fabrication of cross-sectional specimens using a dual-beam instrument (FEI Helios 600i).

Optical Characterization. All the PL, lasing, and TRPL were performed with the confocal μ -PL system (WITec, alpha-300). The CW lasers at 375 and 488 nm were used as the excitation sources for PL measurements of the CsPb(Br_xCl_{1-x})₃ and CsPb(I_{1-x}Br_x)₃ samples, respectively. Both of the two lasers were introduced to the confocal system and focused onto the samples through a 100 \times objective at the top of the samples. The PL signals of each triangular micro/nanorod were collected by the same objective and detected by a CCD spectrometer (600 g/mm grating). Spectra Physics Ti:Sapphire laser at 360 nm (100 fs, 1 kHz) was used for lasing and TRPL measurements. The pumping source was focused obliquely on the sample by a lens.

The TRPL of the triangular micro/nanorods was detected with a streak camera system (Hamamatsu, C10910) with a temporal resolution of about 18 ps.

ASSOCIATED CONTENT

Supporting Information

The Supporting Information is available free of charge on the ACS Publications website at DOI: 10.1021/acsnano.6b07374.

Schematic of the home-built vapor growth system, *in situ* EDX spectra, additional SEM images and optical characterization (PDF)

AUTHOR INFORMATION

Corresponding Authors

*E-mail: xiao_wang@hnu.edu.cn.

*E-mail: anlian.pan@hnu.edu.cn.

ORCID

Anlian Pan: 0000-0003-3335-3067

Notes

The authors declare no competing financial interest.

ACKNOWLEDGMENTS

All authors gratefully acknowledge financial support from the National Natural Science Foundation of China (grant nos. 51302077, 51525202, 61574054, and 11374092), the Hunan Provincial Natural Science Foundation of China (grant no. 2015JJ3049), and the Fundamental Research Funds for the Central Universities for financial support.

REFERENCES

- (1) Xing, G.; Mathews, N.; Lim, S. S.; Yantara, N.; Liu, X.; Sabba, D.; Grätzel, M.; Mhaisalkar, S.; Sum, T. C. Low-Temperature Solution-Processed Wavelength-Tunable Perovskites for Lasing. *Nat. Mater.* **2014**, *13*, 476–480.
- (2) Dong, Q.; Fang, Y.; Shao, Y.; Mulligan, P.; Qiu, J.; Cao, L.; Huang, J. Electron-Hole Diffusion Lengths > 175 μm in Solution-Grown $\text{CH}_3\text{NH}_3\text{PbI}_3$ Single Crystals. *Science* **2015**, *347*, 967–970.
- (3) Sutton, R. J.; Eperon, G. E.; Miranda, L.; Parrott, E. S.; Kamino, B. A.; Patel, J. B.; Horantner, M. T.; Johnston, M. B.; Haghhighrad, A. A.; Moore, D. T.; Snaith, H. J. Bandgap-Tunable Cesium Lead Halide Perovskites with High Thermal Stability for Efficient Solar Cells. *Adv. Energy Mater.* **2016**, *6*, 1502458.
- (4) Song, J.; Li, J.; Li, X.; Xu, L.; Dong, Y.; Zeng, H. Quantum Dot Light-Emitting Diodes Based on Inorganic Perovskite Cesium Lead Halides (CsPbX_3). *Adv. Mater.* **2015**, *27*, 7162–7167.
- (5) Zhu, H.; Fu, Y.; Meng, F.; Wu, X.; Gong, Z.; Ding, Q.; Gustafsson, M. V.; Trinh, M. T.; Jin, S.; Zhu, X.-Y. Lead Halide Perovskite Nanowire Lasers with Low Lasing Thresholds and High Quality Factors. *Nat. Mater.* **2015**, *14*, 636–642.
- (6) Xiao, M.; Huang, F.; Huang, W.; Dkhissi, Y.; Zhu, Y.; Etheridge, J.; Gray-Weale, A.; Bach, U.; Cheng, Y.-B.; Spiccia, L. A. Fast Deposition-Crystallization Procedure for Highly Efficient Lead Iodide Perovskite Thin-Film Solar Cells. *Angew. Chem.* **2014**, *126*, 10056–10061.
- (7) Wang, Y.; Li, X.; Song, J.; Xiao, L.; Zeng, H.; Sun, H. All-Inorganic Colloidal Perovskite Quantum Dots: A New Class of Lasing Materials with Favorable Characteristics. *Adv. Mater.* **2015**, *27*, 7101–7108.
- (8) Yakunin, S.; Protesescu, L.; Krieg, F.; Bodnarchuk, M. I.; Nedelcu, G.; Humer, M.; De Luca, G.; Fiebig, M.; Heiss, W.; Kovalenko, M. V. Low-Threshold Amplified Spontaneous Emission and Lasing from Colloidal Nanocrystals of Caesium Lead Halide Perovskites. *Nat. Commun.* **2015**, *6*, 8056.
- (9) Xing, J.; Liu, X.; Zhang, Q.; Ha, S. T.; Yuan, Y.; Shen, C.; Sum, T. C.; Xiong, Q. Vapor Phase Synthesis of Organometal Halide

Perovskite Nanowires for Tunable Room-Temperature Nanolasers. *Nano Lett.* **2015**, *15*, 4571–4577.

(10) Zhang, Q.; Ha, S. T.; Liu, X.; Sum, T. C.; Xiong, Q. Room-Temperature Near-Infrared High-Q Perovskite Whispering-Gallery Planar Nanolasers. *Nano Lett.* **2014**, *14*, 5995–6001.

(11) Ha, S. T.; Liu, X.; Zhang, Q.; Giovanni, D.; Sum, T. C.; Xiong, Q. Synthesis of Organic–Inorganic Lead Halide Perovskite Nanoplatelets: Towards High-Performance Perovskite Solar Cells and Optoelectronic Devices. *Adv. Opt. Mater.* **2014**, *2*, 838–844.

(12) Akkerman, Q. A.; D’Innocenzo, V.; Accornero, S.; Scarpellini, A.; Petrozza, A.; Prato, M.; Manna, L. Tuning the Optical Properties of Cesium Lead Halide Perovskite Nanocrystals by Anion Exchange Reactions. *J. Am. Chem. Soc.* **2015**, *137*, 10276–10281.

(13) Yettapu, G. R.; Talukdar, D.; Sarkar, S.; Swarnkar, A.; Nag, A.; Ghosh, P.; Mandal, P. Terahertz Conductivity within Colloidal CsPbBr_3 Perovskite Nanocrystals: Remarkably High Carrier Mobilities and Large Diffusion Lengths. *Nano Lett.* **2016**, *16*, 4838–4848.

(14) Liu, Q.; Wang, Y.; Sui, N.; Wang, Y.; Chi, X.; Wang, Q.; Chen, Y.; Ji, W.; Zou, L.; Zhang, H. Exciton Relaxation Dynamics in Photo-Excited CsPbI_3 Perovskite Nanocrystals. *Sci. Rep.* **2016**, *6*, 29442.

(15) Yuan, H.; Debroye, E.; Janssen, K.; Naiki, H.; Steuwe, C.; Lu, G.; Moris, M.; Orgiu, E.; Uji-i, H.; De Schryver, F.; Samorì, P.; Hofkens, J.; Roefsaers, M. Degradation of Methylammonium Lead Iodide Perovskite Structures through Light and Electron Beam Driven Ion Migration. *J. Phys. Chem. Lett.* **2016**, *7*, 561–566.

(16) Li, J.; Bade, S. G. R.; Shan, X.; Yu, Z. Single-Layer Light-Emitting Diodes Using Organometal Halide Perovskite/Poly(Ethylene Oxide) Composite Thin Films. *Adv. Mater.* **2015**, *27*, 5196–5202.

(17) You, J.; Meng, L.; Song, T.-B.; Guo, T.-F.; Yang, Y.; Chang, W.-H.; Hong, Z.; Chen, H.; Zhou, H.; Chen, Q.; Liu, Y.; De Marco, N.; Yang, Y. Improved Air Stability of Perovskite Solar Cells via Solution-Processed Metal Oxide Transport Layers. *Nat. Nanotechnol.* **2016**, *11*, 75–81.

(18) Wang, P.; Bai, X.; Sun, C.; Zhang, X.; Zhang, T.; Zhang, Y. Multicolor Fluorescent Light-Emitting Diodes Based on Cesium Lead Halide Perovskite Quantum Dots. *Appl. Phys. Lett.* **2016**, *109*, 063106.

(19) Ravi, V. K.; Markad, G. B.; Nag, A. Band Edge Energies and Excitonic Transition Probabilities of Colloidal CsPbX_3 ($X = \text{Cl}, \text{Br}, \text{I}$) Perovskite Nanocrystals. *ACS Energy Lett.* **2016**, *1*, 665–671.

(20) Fu, Y.; Zhu, H.; Stoumpos, C. C.; Ding, Q.; Wang, J.; Kanatzidis, M. G.; Zhu, X.; Jin, S. Broad Wavelength Tunable Robust Lasing from Single-Crystal Nanowires of Cesium Lead Halide Perovskites (CsPbX_3 , $X = \text{Cl}, \text{Br}, \text{I}$). *ACS Nano* **2016**, *10*, 7963–7972.

(21) Ren, P.; Hu, W.; Zhang, Q.; Zhu, X.; Zhuang, X.; Ma, L.; Fan, X.; Zhou, H.; Liao, L.; Duan, X.; Pan, A. Band-Selective Infrared Photodetectors with Complete-Composition-Range $\text{InAs}_x\text{P}_{1-x}$ Alloy Nanowires. *Adv. Mater.* **2014**, *26*, 7444–7449.

(22) Gong, Y.; Shi, G.; Zhang, Z.; Zhou, W.; Jung, J.; Gao, W.; Ma, L.; Yang, Y.; Yang, S.; You, G.; Vajtai, R.; Xu, Q.; MacDonald, A. H.; Yakobson, B. I.; Lou, J.; Liu, Z.; Ajayan, P. M. Direct Chemical Conversion of Graphene to Boron- and Nitrogen- and Carbon-Containing Atomic Layers. *Nat. Commun.* **2014**, *5*, 3193.

(23) Nedelcu, G.; Protesescu, L.; Yakunin, S.; Bodnarchuk, M. I.; Grotevent, M. J.; Kovalenko, M. V. Fast Anion-Exchange in Highly Luminescent Nanocrystals of Cesium Lead Halide Perovskites (CsPbX_3 , $X = \text{Cl}, \text{Br}, \text{I}$). *Nano Lett.* **2015**, *15*, 5635–5640.

(24) Weidman, M. C.; Seitz, M.; Stranks, S. D.; Tisdale, W. A. Highly Tunable Colloidal Perovskite Nanoplatelets through Variable Cation, Metal, and Halide Composition. *ACS Nano* **2016**, *10*, 7830–7839.

(25) Lignos, I.; Stavrakis, S.; Nedelcu, G.; Protesescu, L.; deMello, A. J.; Kovalenko, M. V. Synthesis of Cesium Lead Halide Perovskite Nanocrystals in a Droplet-Based Microfluidic Platform: Fast Parametric Space Mapping. *Nano Lett.* **2016**, *16*, 1869–1877.

(26) Zhang, D.; Yang, Y.; Bekenstein, Y.; Yu, Y.; Gibson, N. A.; Wong, A. B.; Eaton, S. W.; Kornienko, N.; Kong, Q.; Lai, M.; Alivisatos, A. P.; Leone, S. R.; Yang, P. Synthesis of Composition Tunable and Highly Luminescent Cesium Lead Halide Nanowires through Anion-Exchange Reactions. *J. Am. Chem. Soc.* **2016**, *138*, 7236–7239.

- (27) Zhang, Q.; Zhu, X.; Li, Y.; Liang, J.; Chen, T.; Fan, P.; Zhou, H.; Hu, W.; Zhuang, X.; Pan, A. Nanolaser Arrays Based on Individual Waved CdS Nanoribbons. *Laser Photonics Rev.* **2016**, *10*, 458–464.
- (28) Gu, F.; Yang, Z.; Yu, H.; Xu, J.; Wang, P.; Tong, L.; Pan, A. Spatial Bandgap Engineering along Single Alloy Nanowires. *J. Am. Chem. Soc.* **2011**, *133*, 2037–2039.
- (29) Eaton, S. W.; Lai, M.; Gibson, N. A.; Wong, A. B.; Dou, L.; Ma, J.; Wang, L. W.; Leone, S. R.; Yang, P. Lasing in Robust Cesium Lead Halide Perovskite Nanowires. *Proc. Natl. Acad. Sci. U. S. A.* **2016**, *113*, 1993–1998.
- (30) Wang, Y.; Li, X.; Zhao, X.; Xiao, L.; Zeng, H.; Sun, H. Nonlinear Absorption and Low-Threshold Multiphoton Pumped Stimulated Emission from All-Inorganic Perovskite Nanocrystals. *Nano Lett.* **2016**, *16*, 448–453.
- (31) Guo, P.; Zhuang, X.; Xu, J.; Zhang, Q.; Hu, W.; Zhu, X.; Wang, X.; Wan, Q.; He, P.; Zhou, H.; Pan, A. Low-Threshold Nanowire Laser Based on Composition-Symmetric Semiconductor Nanowires. *Nano Lett.* **2013**, *13*, 1251–1256.
- (32) Zhang, Q.; Su, R.; Liu, X.; Xing, J.; Sum, T. C.; Xiong, Q. High-Quality Whispering-Gallery-Mode Lasing from Cesium Lead Halide Perovskite Nanoplatelets. *Adv. Funct. Mater.* **2016**, *26*, 6238–6245.
- (33) Park, K.; Lee, J. W.; Kim, J. D.; Han, N. S.; Jang, D. M.; Jeong, S.; Park, J.; Song, J. K. Light–Matter Interactions in Cesium Lead Halide Perovskite Nanowire Lasers. *J. Phys. Chem. Lett.* **2016**, *7*, 3703–3710.
- (34) Gradečak, S.; Qian, F.; Li, Y.; Park, H.-G.; Lieber, C. M. GaN Nanowire Lasers with Low Lasing Thresholds. *Appl. Phys. Lett.* **2005**, *87*, 173111.
- (35) Moller, C. K. Crystal Structure and Photoconductivity of Caesium Plumbohalides. *Nature* **1958**, *182*, 1436–1436.
- (36) Beal, R. E.; Slotcavage, D. J.; Leijtens, T.; Bowring, A. R.; Belisle, R. A.; Nguyen, W. H.; Burkhard, G. F.; Hoke, E. T.; McGehee, M. D. Cesium Lead Halide Perovskites with Improved Stability for Tandem Solar Cells. *J. Phys. Chem. Lett.* **2016**, *7*, 746–751.
- (37) Li, X.; Wu, Y.; Zhang, S.; Cai, B.; Gu, Y.; Song, J.; Zeng, H. CsPbX₃ Quantum Dots for Lighting and Displays: Room-Temperature Synthesis, Photoluminescence Superiorities, Underlying Origins and White Light-Emitting Diodes. *Adv. Funct. Mater.* **2016**, *26*, 2435–2445.
- (38) Protesescu, L.; Yakunin, S.; Bodnarchuk, M. I.; Krieg, F.; Caputo, R.; Hendon, C. H.; Yang, R. X.; Walsh, A.; Kovalenko, M. V. Nanocrystals of Cesium Lead Halide Perovskites (CsPbX₃, X = Cl, Br, and I): Novel Optoelectronic Materials Showing Bright Emission with Wide Color Gamut. *Nano Lett.* **2015**, *15*, 3692–3696.
- (39) Niu, G.; Yu, H.; Li, J.; Wang, D.; Wang, L. Controlled Orientation of Perovskite Films through Mixed Cations toward High Performance Perovskite Solar Cells. *Nano Energy* **2016**, *27*, 87–94.
- (40) Yin, W.-J.; Yan, Y.; Wei, S.-H. Anomalous Alloy Properties in Mixed Halide Perovskites. *J. Phys. Chem. Lett.* **2014**, *5*, 3625–3631.
- (41) Casperson, L. W. Threshold Characteristics of Multimode Laser Oscillators. *J. Appl. Phys.* **1975**, *46*, 5194–5201.
- (42) Tanner, S. M.; Gray, J. M.; Rogers, C. T.; Bertness, K. A.; Sanford, N. A. High-Q GaN Nanowire Resonators and Oscillators. *Appl. Phys. Lett.* **2007**, *91*, 203117.
- (43) Zhang, Q.; Li, G.; Liu, X.; Qian, F.; Li, Y.; Sum, T. C.; Lieber, C. M.; Xiong, Q. A Room Temperature Low-Threshold Ultraviolet Plasmonic Nanolaser. *Nat. Commun.* **2014**, *5*, 4953.
- (44) Piccione, B.; Cho, C.-H.; van Vugt, L. K.; Agarwal, R. All-Optical Active Switching in Individual Semiconductor Nanowires. *Nat. Nanotechnol.* **2012**, *7*, 640–645.
- (45) Xu, J.; Ma, L.; Guo, P.; Zhuang, X.; Zhu, X.; Hu, W.; Duan, X.; Pan, A. Room-Temperature Dual-Wavelength Lasing from Single-Nanoribbon Lateral Heterostructures. *J. Am. Chem. Soc.* **2012**, *134*, 12394–12397.
- (46) Samuel, I. D. W.; Nanddas, E. B.; Turnbull, G. A. How to Recognize Lasing. *Nat. Photonics* **2009**, *3*, 546–549.
- (47) Pan, A.; Liu, R.; Yang, Q.; Zhu, Y.; Yang, G.; Zou, B.; Chen, K. Stimulated Emissions in Aligned CdS Nanowires at Room Temperature. *J. Phys. Chem. B* **2005**, *109*, 24268–24272.
- (48) Zou, B.; Liu, R.; Wang, F.; Pan, A.; Cao, L.; Wang, Z. L. Lasing Mechanism of ZnO Nanowires/Nanobelts at Room Temperature. *J. Phys. Chem. B* **2006**, *110*, 12865–12873.
- (49) Johnson, J. C.; Knutsen, K. P.; Yan, H.; Law, M.; Zhang, Y.; Yang, P.; Saykally, R. J. Ultrafast Carrier Dynamics in Single ZnO Nanowire and Nanoribbon Lasers. *Nano Lett.* **2004**, *4*, 197–204.